Contents lists available at ScienceDirect

Remote Sensing of Environment

LandTrendr smoothed spectral profiles enhance woody encroachment monitoring

P.J. Gelabert [a,b,*], M. Rodrigues [a,b], J. de la Riva [c], A. Ameztegui [a,b], M.T. Sebastià [d,e], C. Vega-Garcia [a,b]

[a] Department of Agricultural and Forest Engineering, University of Lleida, Alcalde Rovira Roure 191, 25198 Lleida, Spain
[b] Joint Research Unit CTFC-Agrotecnio, Ctra. Sant Llorenç km.2, 25280 Solsona, Spain
[c] GEOFOREST-IUCA, Department of Geography and Land Management, C/ Pedro Cerbuna 12, 50009 Zaragoza, Spain
[d] Group GAMES and Department of Horticulture, Botany and Landscaping, School of Agrifood and Forestry Science and Engineering, University of Lleida, Alcalde Rovira Roure 191, 25198 Lleida, Spain
[e] Laboratory of Functional Ecology and Global Change (ECOFUN), Forest Sciences Centre of Catalonia (CTFC), Ctra. Sant Llorenç km.2, 25280 Solsona, Spain

ARTICLE INFO

ABSTRACT

Secondary succession (SS) is one of the main consequences of the abandonment of agricultural and forestry practices in rural areas, causing -among other processes- woody encroachment on former pastures and croplands. In this study we model and monitor the spatial evolution of SS over semi-natural grassland communities in the mountain range of the Pyrenees in Spain, during the last 36 years (1984-2019). Independent variables for 'annual-based' and 'period-based' modeling were drawn from a suite of Surface Reflectance Landsat images, LandTrendr (LT)-algorithm-adjusted images and LT outputs. Support vector machine (SVM) classifiers were trained and tested using all possible variable combinations of all the aforementioned datasets. The best modeling strategy involved yearly time series of LT-adjusted Tasseled Cap Brightness (TCB) and Wetness (TCW) axes as predictors, attaining a F1-score of 0.85, a Matthew Correlation Coefficient (MCC) of 0.67 and an AUC 0.83. Woodlands encroached above 480,000 ha of grasslands and crops during the study period. A model using LT outputs for the whole period also denoted good performance (F1-score = 0.85, MCC = 0.75) and estimated a similar area of woodland expansion (~509,000 ha), but this 'period' approach was unable to provide temporal information on the year or the encroachment dynamics. Our results suggest an overall proportion of 66% for the Pyrenees being affected by SS, with higher intensity in the west-central part, decreasing towards the eastern end.

1. Introduction

Global change promotes swift environmental responses through sharp socio-economic and environmental dynamics (Lahsen et al., 2010), leading to land cover transformations such as those triggered by land abandonment.

Grassland communities are among the most extended biomes around the world (Ali et al., 2016; Latham et al., 2014), and are an important food provider for humans through livestock grazing. Livestock transform forages not suitable for human consumption into food such as milk and meat (O'Mara, 2012), accounting for up to 27% of the global meat supply in 2018 (FAO, 2018). Natural grasslands such as savannah or steppes cover vast areas in Asia, Africa, America and Australia, whereas managed and semi-natural grasslands are predominant in Europe and

North America (Foley et al., 2005; O'Mara, 2012).

In Europe, semi-natural grasslands extend over large areas in the Central and Eastern plains, the British islands and the Mediterranean basin (Foley et al., 2005). In all European countries, the abandonment of traditional agricultural practices (e.g., free-ranging livestock, and sheep- or cattle-grazed rainfed crops) since the 1950's has led to the pervasive loss of semi-natural grasslands, colonized by shrub and tree communities in an ecological process known as secondary succession (SS). Land abandonment and SS have particularly affected mountain areas (Lasanta et al., 2017), and have both positive and negative side effects (Ustaoglu and Collier, 2018). The most widely recognized positive impact is carbon sequestration (Navarro and Pereira, 2012), though some recent studies suggest the expansion of shrubland-type communities may reduce the overall carbon pool at the ecosystem level (e.g. Sørensen

---

et al., 2018). Well-managed grasslands also act as CO_2 sinks, with considerable potential for soil organic carbon storage (0.01 to 0.3 Gt C yr^{-1}; Lal, 2004). On the negative side, biodiversity usually decline after woody encroachment (Van Auken, 2009), as do water availability and river flow. Potential undesired effects, including biodiversity loss, damage to ecosystem services, fuel built-up, or land degradation, are often a consequence of the withdrawal of human stewardship that has kept these cultural landscapes open. In fire-prone ecosystems, the SS process increases wildfire hazard due to fuel accumulation (Lasanta et al., 2018; Pausas and Bond, 2020).

Monitoring the evolution of SS contributes to a better understanding of its drivers and ecological implications, while being a helpful source of information for environmental assessment, decision-making and planning. Remote Sensing (RS) is both a powerful tool and a valuable resource to assess land cover dynamics at multiple scales. Satellite imagery has been extensively used to monitor land cover change (Turner et al., 1994), particularly SS following land abandonment. Without being exhaustive, we found examples in eastern Europe (Baumann et al., 2011; Kuemmerle et al., 2009; Kuemmerle et al., 2008), or the entire European continent (Alcantara et al., 2012; Estel et al., 2015).

Though threatened by SS after land abandonment, sub-alpine grasslands in the central and eastern Pyrenees are one of the larger hotspots of managed grasslands in the world (Ali et al., 2016). In the Pyrenees, experiences on SS monitoring are scarce to date (Gartzia et al., 2014; José Vidal-Macua et al., 2017) and mostly limited to the local scale (valley or watershed). Several studies in the Spanish Pyrenees have assessed SS based on visual photointerpretation (Améztegui et al., 2010; Cervera et al., 2019; Mottet et al., 2006; Poyatos et al., 2003) or temporal trends of spectral indices (Lasanta and Vicente-Serrano, 2007; Vicente-Serrano et al., 2006). In the French Pyrenees, Vacquie et al. (2015) analyzed future land use changes at regional level under different scenarios. Nonetheless, to date there is no comprehensive analysis of the spatial and temporal evolution of SS over the highly diverse and valuable managed grasslands covering the entire range of the Spanish Pyrenees.

In this study, we developed and exemplified a methodological procedure to assess and monitor the dynamic of SS. To do so, we leveraged the LandTrendr algorithm (LT; Kennedy et al., 2010), an innovative technique specifically designed to detect land cover changes. According to Kennedy et al. (2010) there are two broad types of change detection procedures using RS. One focuses on identifying deviations on the spectral signal (e.g. Vegetation Change Tracker (VCT) (Huang et al., 2010) and Continuous Change Detection and Classification (CCDC) (Zhu and Woodcock, 2014); the second approach isolates changes in time-series by fitting smoothing algorithms to simplify chronosequences into representative temporal trajectories. LT, which falls within the later approach, uses a set of spectral-temporal segmentation algorithms optimized for Landsat imagery, allowing the detection of changes in the Earth's surface (Kennedy et al., 2010). LT computes trajectory-based spectral data series, omitting or at least significantly reducing the noise in the spectral signal (Kennedy et al., 2010). Former applications of LT have addressed forest changes and disturbance detection (Cohen et al., 2018; Kennedy et al., 2012; Kennedy et al., 2010; Senf et al., 2015) or general land cover change (Franklin et al., 2015), but SS of grassland ecosystems after abandonment remains unexplored. SS develops over decades, with the additional technical challenge posed in our study by the topographic and socioeconomic complex mountain environment of the Pyrenees. In this work, we applied LT to the complete series of Landsat images (1984–2019) using the Google Earth Engine platform. We combined RS imagery with highly detailed (1:25,000) land cover maps and aerial ortophotography by means of machine learning algorithms to (i) compare the performance of raw spectral indices, LT trajectories and LT outputs in monitoring grassland losses at regional and local scales and, (ii) develop a reliable procedure to detect and map SS over 36 years (1984–2019).

2. Study area

The study region covers the Spanish side of the Pyrenees mountain range (Fig. 1). The Pyrenees extend over a 400 km range over the Iberian Peninsula isthmus between Spain and France. It is the second highest mountain system in the Iberian Peninsula (500 to 3400 m.a.s.l.). The climate is high mountain microclimate with oceanic influence at the western part, with rainfall accumulation varying across an altitudinal gradient and ranging from 700 to 2500 mm/yr, and mean annual temperatures from 4 to 8 °C (Cuadrat et al., 2007). Crops and grasslands cover approximately 10% of the Pyrenees (SIOSE, 2014), with environmental conditions favoring a wide spectrum of vegetation species and communities, arranged in elevation belts. Herbaceous crops are cultivated in lowlands, sometimes combined with woody crops in the southern part. Above 1600 m.a.s.l. the temperature conditions do not allow cereal growing, being predominant natural and managed grasslands/pastures (García Ruiz and Lasanta, 2018) combined mainly with mountain pine (*Pinus uncinata* Ramond ex A.DC.) forests. In forested montane belt areas (600–1600 m.a.s.l.) beech (*Fagus sylvatica* L.) and fir (*Albies alba* Mill.) predominate in shaded aspects.

During the last decades, the agrarian economic sector was progressively replaced by tourism activities transforming economy, landscape and demographic trends (Lasanta et al., 2013). This reduction is evidenced by the reduction of livestock units between 1999 and 2009, with a decrease of 77,000 units (−12%) (INE, 2009; INE, 1999). Specifically, there was a drastic reduction of goat and sheep cattle, and a slight increase of cows and horses, being the last one a special case of breed for recreational purposes.

3. Methods

The identification of areas that experienced SS was based on the combination of land cover information and RS imagery. We developed two modeling approaches, one based on the temporal ('annual-based') progression of land cover types characterizing SS (grasslands and woodlands) and a second that distinguished areas historically affected by SS from those with persistent grassland communities ('period-based'). The first approach leveraged time series of spectral imagery while the second relied on complex spectral indices of magnitude and direction of change in the spectral response. Remote sensing imagery and spectral indices were accessed and built using the Google Earth Engine platform (GEE; Gorelick et al., 2017) and the LT algorithm (Kennedy et al., 2018; Kennedy et al., 2010). Statistical analyses and models were conducted using the R software (R Core Team, 2017).

3.1. Response variables

3.1.1. Grassland versus woody communities
Land cover types involved in SS, i.e., all grasslands types and woody vegetation communities, were retrieved from the Spanish Land Cover Information System (SIOSE). The SIOSE dataset provided highly accurate (1:25,000 scale) land cover information for recent years (2005, 2009, 2011 and 2014), but not for the whole study period (1984-2019). We used the latest version of SIOSE (2014) to retrieve the most up-to-date spatial distribution of croplands and grasslands (categories 212 [Herbaceous crops], 290 [Pastures] and 300 [Grasslands]), shrublands (320) and forested areas (311 [Hardwood], 312 [Deciduous], 313 [Evergreen] and 316 [Coniferous]). Water layers (514 [Reservoir], 511 [Rivers], 512 [Lagoons], 513 [Lakes] and 411 [Swamps]), bare ground (354 [Quaternary lava washes], 352 [Rocky outcrop]) and urban areas (111 [Urban continuous], 112 [Urban discontinuous] and 113 [Other urban areas]) were excluded from further analyses. This information was used to model the temporal evolution of SS as described in Section 3.3.1.

Fig. 1. Study area. Hillshade is used as background.

3.1.2. Evidence of SS

In order to obtain 'ground truth' information to discriminate encroached sites from persistent grassland communities over the whole study period, we carried out a photointerpretation of the available historical series of aerial orthophotography in Spain, longer than the SIOSE dataset. The main goal was identifying areas that transitioned anytime in 1984-2019 from 'grassland or cropland' into 'woodland' (either scrublands, trees or both) to serve as test sample for the evaluation of model performance. We built a complementary modeling procedure upon this information by training and testing binary models for the whole period based on historical evidence of SS opposed to locations with persistent grasslands (see Section 3.3.2).

From the collection of orthophotographs, we were able to identify a set of 477 locations including 250 sites not experiencing SS and 227 locations affected by SS. We visually analyzed and digitized sites in the series of orthophotographs provided by the Spanish Geographic Institute (IGN) from the National Plan of Aerial Orthophotography (PNOA, 2019), the OLISAT project (1997/1998) and the SIGPAC (1997/2003). Digital orthophotographs were supplied via the Spatial Data Infrastructure of Navarra (IDENA), Catalonia (ICGC) and the Spanish Geographical Institute (IGN). Table 1 provides information on these sources of aerial orthophotography. The selection of sampling sites was based on a systematic approach guided by a 5 × 5 km grid covering the entire study area. Each grid point was visually inspected to determine whether it experienced SS any time during the period of analysis.

Table 1
Description of aerial orthophotography datasets used in this study.

Extent	Server	Project/ program	Scale	Resolution	Year
Spain	IGN	PNOA	1:15,000	0.25 m	2017–2018
Spain	IGN	OLISAT	1:30,000	0.50 m	1997 & 1999
Spain	IGN	SIGPAC	1:40,000	0.50 m	1997, 2002 & 2003
Catalonia	ICGC	–	1:5000	0.50 m	1988
Navarra	IDENA	–	1:5000	0.50 m	1982

3.2. Spectral response of the land cover

Models to identify SS were trained from land cover based data and the spectral signal of the land cover. A set of Landsat TM, ETM+ and OLI surface reflectance images (SR images) for spring (March-May, 213 images), summer (June-August, 216) and autumn (September-November, 213) were used in our analyses. We retrieved and processed images via the GEE environment (Gorelick et al., 2017) Tier 1 surface reflectance collection in the period 1984 to 2019, covering the region between paths 197 to 200 and rows 30 and 31. First, we homogenized OLI data to be comparable with TM/ETM+ sensors data, images were transformed as suggested by Roy et al. (2016). Then, we calculated the band value annual medoid at pixel level on a seasonal basis.

3.2.1. Image pre-processing and preparation

The Tasseled Cap transformation (TC; Crist and Cicone, 1984) was applied to synthetize the original set of 6 spectral bands into a smaller subset of covariates. TC is an orthogonal transformation of spectral data based on the 'physical-sense' of the 3 resulting axes: brightness (TCB), greenness (TCG) and wetness (TCW). Time series of the 3 components transformation (further referred to as TC Raw) were obtained applying the weighting scheme (Table 1 – supplementary material) proposed by Crist (1985). As aforementioned, the spectral information from TM and ETM+ images was homogenized using the procedure described by Roy et al. (2016). The procedure allows applying the same weights to images from either TM, ETM+ or OLI sensors.

The Tasseled Cap Angle (TCA) was also calculated as the angle formed by the TCG and TCB axes (Eq. (1)). It works as a proxy of the vegetation plane (Crist and Cicone, 1984), i.e., the proportion of vegetation to non-vegetation (Gómez et al., 2011).

$$TCA = arctan\left(\frac{TCG}{TCB}\right) \qquad (1)$$

3.2.2. LT processing

TC time series were submitted to the LT algorithm. LT consists of a series of spectral-temporal segmentation algorithms to isolate changes

in time series. Generally speaking, the trajectories in the original time series were iteratively simplified by identifying the key vertexes of change. Potential vertexes were identified and linked using flexible fitting rules, and then different segments in the updated trajectory were removed and remodeled to ultimately pick the best model (Kennedy et al., 2010). We used the GEE's version of LT as implemented by Kennedy et al. (2018). Processing data with GEE significantly reduced computational time consumption while ensuring the replicability of the procedure elsewhere (Gorelick et al., 2017). The LT algorithm was applied to get fitted-to-vertex time series for every pixel and TC component (further referred to as LTTC). Furthermore, we also retrieved LT's change detection outputs (change magnitude, pre-change value and change duration) for each TC input (LT outputs). Change magnitude relates to the highest difference between two vertexes. Pre-change refers to the initial or starting value in a trajectory. Change duration denotes the slowest change in a given trajectory (usually gain in TCA, TCG, TCW and decline in TCB). We obtained it sorting by the slowest gain and the slowest loss for each TC. After that, in a subsequent process, we selected the magnitude of change and merge loss and gain outputs filtering overlaps by the slowest change.

3.3. Classification models

In order to identify areas experiencing SS, we applied the Support Vector Machine (SVM) classification algorithm. Among the machine learning algorithms, SVM has been reported to better discriminate into binary categories (Rodrigues and de la Riva, 2014) being frequently used to model agricultural abandonment (Alcantara et al., 2012; Kuemmerle et al., 2008). SVM has been specifically designed to analyze and recognize patterns. It is based on the constructing of a set of hyperplanes in a high-dimensional space searching for the maximum separability between classes (Cortes and Vapnik, 1995; Vapnik, 1998; Vapnik, 1995). SVM parameters must be optimized, selecting the combination of hyperparameters that achieved the highest classification accuracy (see Sections 3.3.1 and 3.3.2). We used a *Radial Basis Function* (RBF) kernel, the most commonly applied strategy in land cover classification due to its good performance (Noi and Kappas, 2018). *Cost* and *gamma* parameters were tuned exploring all values ranging from 1 to 700 and 0.001–1, respectively. Model optimization was conducted using a 10-fold cross validation as implemented in the "*caret*" package (Kuhn, 2008). In addition, we used the "*raster*" package (Hijmans, 2019) to generate spatial predictions and outputs.

3.3.1. Modeling the annual progression of SS

This approach aimed at monitoring the temporal evolution of SS year by year, thus enabling to ascertain both when and where SS took place. The method was developed in two stages. First, we calibrated 'grassland' vs 'woodland' classification models from TC axes on a single year (2014); and then we predicted the spatial distribution of 'grassland' vs 'woodland' in the entire time series (1984-2019). To do so, we built a response variable consisting on a binary 'grassland' vs 'woodland' categorical variable, created from SIOSE 2014 (see Section 3.1.1). To ensure consistency with the land cover dataset used to construct the response variable, models were trained using imagery in 2014. Models were built using a training sample of 2878 locations, accounting for 75% of the SIOSE 2014 sample, (1039 pastures and grasslands; 1839 areas with tree and/or shrublands). A total of 56 models were calibrated, resulting from the combination of 3 seasons (spring, summer and fall), 9 possible permutations of TC outputs, avoiding overlapping of TCA with TCB and TCG, and exploring both TC Raw values and LTTCs trajectories. The comparison between using raw values or fitted trajectories was a particular goal of this classification approach.

The second stage of this approach addressed the performance assessment, characterization and mapping of locations experiencing SS. We aimed at determining when SS did occur based on the predicted evolution of 'grassland' and 'woodland'. We inspected the 54 annual time series of classified images, labeling as affected by SS those pixels initially categorized as 'grassland' that were later predicted to be 'woodland'. To account for potential uncertainty due to variability or noise in the spectral signal, we examined the temporal consistency in the classification. That is, for those pixels tagged as affected by SS we estimated a persistence index (PI). The PI was calculated as the ratio between the times (years) 'woodland' was predicted and the number of remaining images (Eq. (2)) after the first prediction of SS. From a theoretical standpoint, PI values ranged from 0 to 1; a PI value of 0 indicated no chance of SS while 1 indicated certain occurrence of SS. Values between 0 and 1 informed on the chance of SS, i.e., the consistency with which 'woodland' was subsequently predicted after the first detection. The PI may be understood as a fuzzy classification approach in which each pixel was assigned a likelihood value; the higher the PI, the more likely SS actually happened.

$$PI = \frac{\sum_{y_{ss}}^{y_f} p_{y_{ss}}}{\sum_{y_{ss}}^{y_f} p} \tag{2}$$

where *PI* is the persistence index; y_{ss} is the first year when SS is predicted; y_f is the last year of the time series; $p_{y_{ss}}$ is a pixel being predicted as affected by SS.

Determining which pixels must be ultimately labeled as affected by SS depended on the PI value. In order to obtain the most reliable SS classification and inform about the sensitivity to the PI threshold (i.e., the value of PI above which we label a given pixel as SS) we conducted a validation and model selection procedure based on the calculation of F1-score (F1) (Chinchor, 1992) in the classification (including commission and omission errors), Mathew Correlation Coefficient (MCC) (Matthews, 1975) and the Area Under the Receiver Operating Characteristic Curve (AUC). Performance indexes were calculated from data described in Section 3.1.2 (Orthophotography-derived dataset, not used for model building), explored along the continuum of all possible thresholds in the range 0-1. The optimal threshold was obtained using the best separability point from AUC (Specificity equal to Sensitivity).

Given the temporal nature of the procedure, PI values were influenced by the time of detection, involving different sample sizes depending on the year were SS was first predicted. For example, the PI of a pixel where SS started in 2000 would be calculated upon 15 records of yearly classification data whereas in a pixel detected in 2017, PI would be calculated with just the 2 remaining years of information. To evidence this potential issue we reported the year when SS was predicted, labelled as 'year of change'. This procedure resulted in two raster layers, one layer gathering the spatial distribution of the PI and a second layer including the year of SS occurrence.

3.3.2. Modeling the 'period-based' progression of SS

The 'period-based' classification approach leveraged LT outputs (see Section 3.2.2) to identify locations affected by SS at any stage during the period 1984-2019. Contrary to the former classification system, this procedure focused on obtaining a 'static' classification of SS, rather than its temporal evolution. Again, a SVM model was trained and tested. The response variable was created from the aerial orthophotography dataset (see Section 3.1.2). We used 80% of the data (198 non-affected locations and 175 areas affected by SS) to train the SVM model and the remaining 20% of the locations to test the model (52 non-affected by SS and 42 experiencing SS). Instead of temporal series of TC components, we calibrated the model from LT outputs calculated in TCB, TCG, TCW and TCA. Again, we explored several combinations of predictors, reporting their performance according to percent accuracy and Cohen's Kappa.

4. Results

4.1. Spatial distribution of SS

TC Raw and LTTC models performed well in monitoring SS. Out of the 54 possible combinations of variables, several models achieved a satisfactory classification accuracy (Table 2, supplementary material). The most successful combination was obtained with LTTC fitted components in spring, requiring only TCW and TCB as predictors (tied if only TCB used). Overall, models calibrated from LTTC chronosequences outperformed their TC Raw counterparts, though by a slim margin. Note that the best combination of variables in TC Raw coincides with that of LTTC but in summertime. Likewise, spring and summer models tended to work best, with fall models attaining 3% less accuracy on average.

The monitoring of areas affected by SS using the temporal approach was conducted using an optimal PI of 0, as suggested by the sensitivity analysis (Fig. 2B). The LTTC and TC raw models were rather insensitive to changes in the PI, though its performance slightly dropped as the PI increased in TC raw. The classification accuracy of the best TC raw model was lower than its LTTC counterpart at any PI threshold. Noticeably, the omission error escalated drastically as the PI threshold increased in the TC raw model (Fig. 2A).

The comparison of the models' performance in identifying SS evidenced the LTTC approach as the best strategy (Table 2). LTTC attained a predictive F1-score of 0.85, a MCC of 0.67 and an AUC of 0.83, estimating an affected extension of 479,703 ha, representing an encroachment of 66% of former grasslands (herbaceous crops and grasslands) by woody species. Commission and omission errors stood at 0.06 and 0.29, respectively. The classification accuracy of LTTC was notably higher than TC Raw's (F1 = 0.79, MCC = 0.54 and AUC = 0.75) predicting an affected area of 508,840 ha (≈70% of analyzed area). Likewise, LTTC outperformed the LT output approach (F1 = 0.71 and MCC = 0.61), with an encroached area of 533,043 ha representing 74% of the grasslands in the study area. None of the 14 models from LT outputs combinations (see Table 3 - supplementary materials) achieved a higher accuracy than the best LTTC. Nonetheless, as in LTTC models, the strongest spectral predictors were the TCB and TCW components. Table 2 summarizes the performances of the three modeling approaches on the validation dataset (ground truth obtained by orthophotography).

From a spatial standpoint, the LTTC approach seemed to capture best the spatial and temporal coverage of the SS phenomena (Figs. 3–5). As observed in Fig. 3B, SS took place earlier in the southwestern end, advancing progressively from valleys to the top of the mountain range. Even though it gave no information on SS temporal progression, the pattern obtained with LT outputs resembled that from LTTC (Fig. 3A). TC Raw models seemed to overestimate the spatial extent of SS while not revealing clear temporal patterns.

4.2. Temporal evolution of SS

The analysis of the temporal distribution of SS, extracted from the LTTC cartographical output (Fig. 3B), along the period 1984-2019 revealed a non-stationary profile in the temporal dynamics: encroachment rates were not steady. The major progression was observed during the 80's decade, decreasing sharply until 1990, and remaining stationary afterward. During the 80's the average annual surface experiencing SS was of approximately 39,000 ha/yr, declining from over 60,000 ha between 1984 and 1985 to less than 10,000 ha in 1990. Since 1990 the average affected area stayed at 7200 ha/yr, descending to 6000 ha/yr over the 20th century (Fig. 6).

5. Discussion

We successfully evaluated a wide array of RS inputs and analysis techniques to identify the best methodology to monitor and assess the occurrence and extent of SS after rural abandonment in mountainous areas, an environmental process with high potential impacts on ecosystem services like biodiversity, fire hazard or carbon balances. The proposed procedure was exemplified in the Spanish Pyrenees, assessing the occurrence of SS over a period of 36 years using the complete series of available Landsat imagery.

LT-based models (LTTC and LT outputs) attained an outstanding performance (Figs. 3 and 5) compared to those calibrated from raw spectral information (TC Raw), either in terms of overall accuracy or commission and omission errors (Table 2). Using LT fitted spectral information significantly reduced noise from differences in illumination conditions, phenological changes, atmospheric conditions, or geometric registration (Kennedy et al., 2010). Despite the fact that both LTTC and LT outputs models showed very good accuracy in detecting spatial patterns of SS (Figs. 3 and 5), the highest accuracy was obtained using LTTC (Table 2). LT-based methods predicted 464,626 (64% of former grasslands) and 533.043 ha (77%) experiencing SS in the period 1984-2019, using LTTC and LC Outputs, respectively. TC Raw models seemed to overestimate the surface affected by SS (commission error = 0.34). According to prior local experiences, 70-80% of the lands were abandoned in Central Pyrenees (both Spanish and French sides). In the Eastern Pyrenees, 36% of the cultivated land were abandoned between 1993 and 2005 (Badia et al., 2014). The reported rates of land abandonment in the Eastern Pyrenees were quite dissimilar, ranging between 96% in Alta Garrotxa (Vila Subirós et al., 2009) and 25% in Cal Rodó (Poyatos et al., 2003).

The most accurate strategy involved LTTC fitted images using the TCB and TCW components. Both TCB and TCW are known to be suitable indicators to discriminate wooded from non-wooded land covers (Frazier et al., 2015). Dense forest communities and, to a lesser extent shrublands, are broadly characterized by higher TCW (increased ability to retain moisture due to shadowing on the understory) and lower TCB values (reduced albedo by lambertian shading due to the rougher texture of the surface) when compared to open stands (Healey et al., 2005). The performance of models including TCG was usually poor, but TCG is considered a weak driver of structural differences (grass, shrub or tree) between forest communities (Frazier et al., 2015; Pickell et al., 2016). Above a threshold of certain biomass density or leaf area, greenness-related indexes do not capture significant differences between vegetation communities (Pickell et al., 2016; Tanase et al., 2011). Models incorporating the combination of TCG and TCB via TCA did not

Table 2

Confusion matrix and performance assessment of the proposed modeling approaches.

	LTTC			TC Raw			LT Outputs		
	Non-SS	SS	Total	Non-SS	SS	Total	Non-SS	SS	Total
Non-SS	230	15	245	200	46	246	41	8	49
SS	64	153	217	60	157	217	10	33	43
Total	294	168		260	203		51	41	
	F1 = 0.85	C = 0.06		F1 = 0.79	C = 0.28		F1 = 0.81	C = 0.16	
	MCC = 0.67	O = 0.29		MCC = 0.54	O = 0.19		MCC = 0.61	O = 0.23	
	SS area: 479,703 ha			SS area: 508,840 ha			SS area: 533,043 ha		

F1; MCC;; C: commission error; O: omission error; SS area: predicted surface of SS.
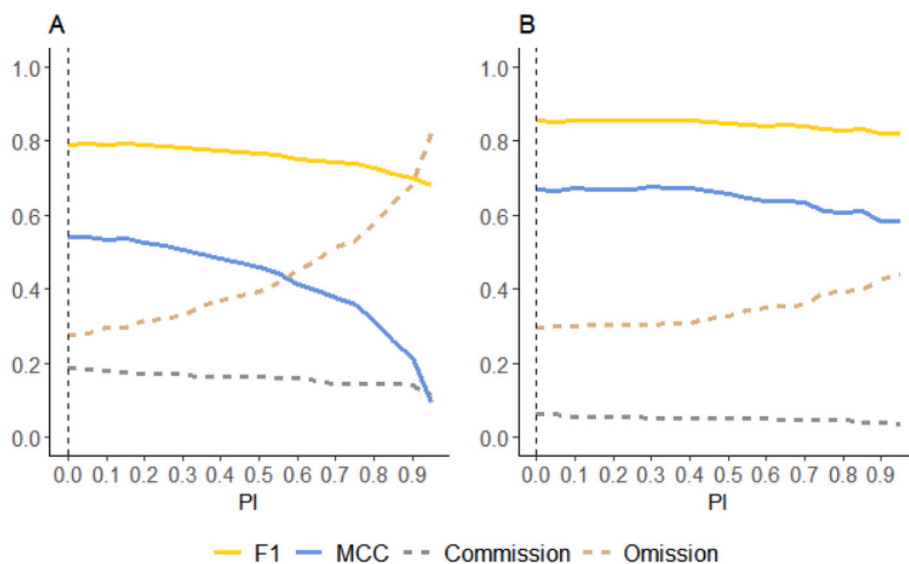
Fig. 2. Sensitivity analysis of 'annual-based' modeling strategies to the PI threshold. The vertical dashed line represents the lower limit of the best PI threshold. A: TC raw model and B: LTTC model.
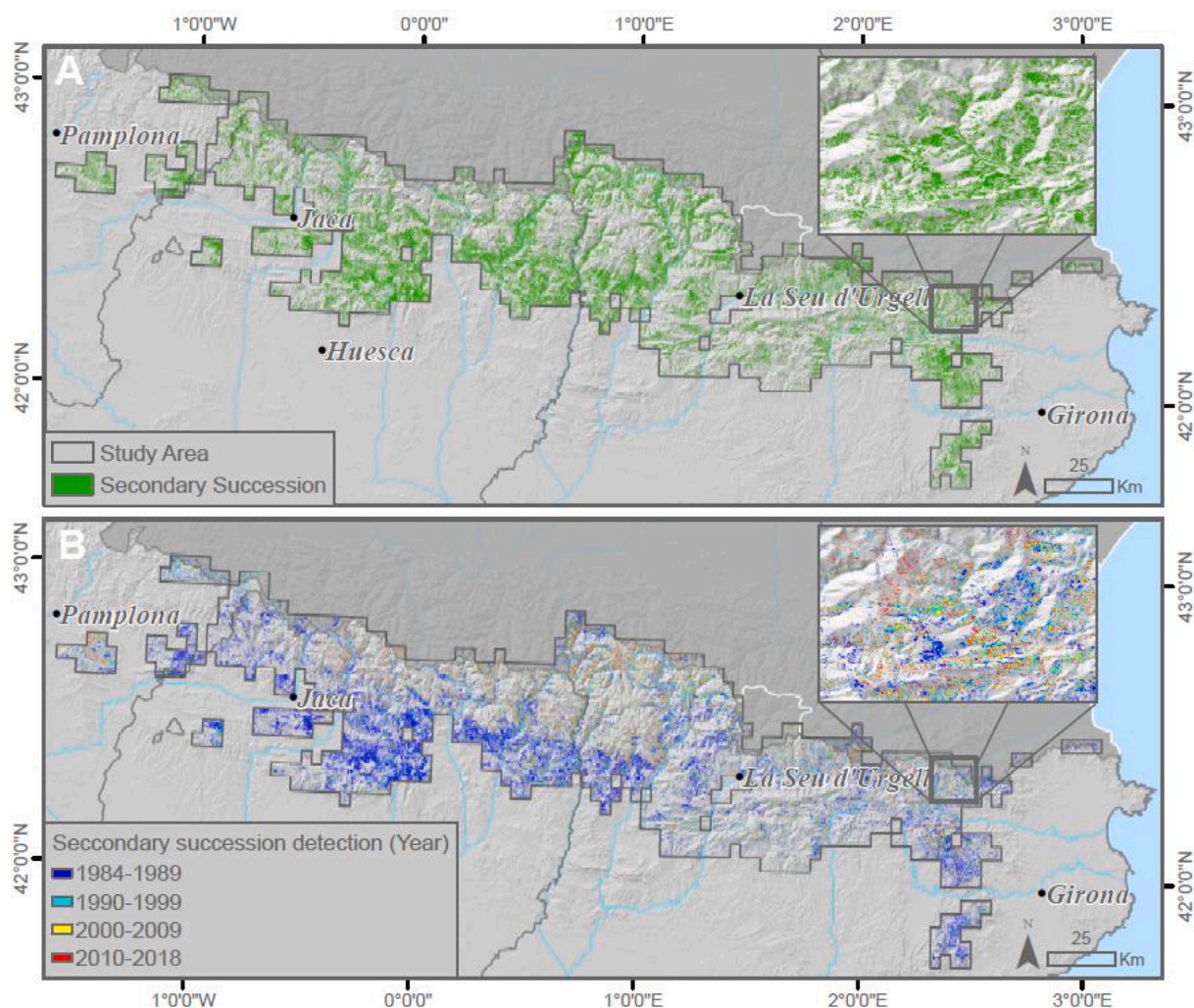

Fig. 3. a) Areas affected by SS using LTTC fitted images; b) Areas affected by SS per year using LTTC fitted images. Hillshade is used as background.
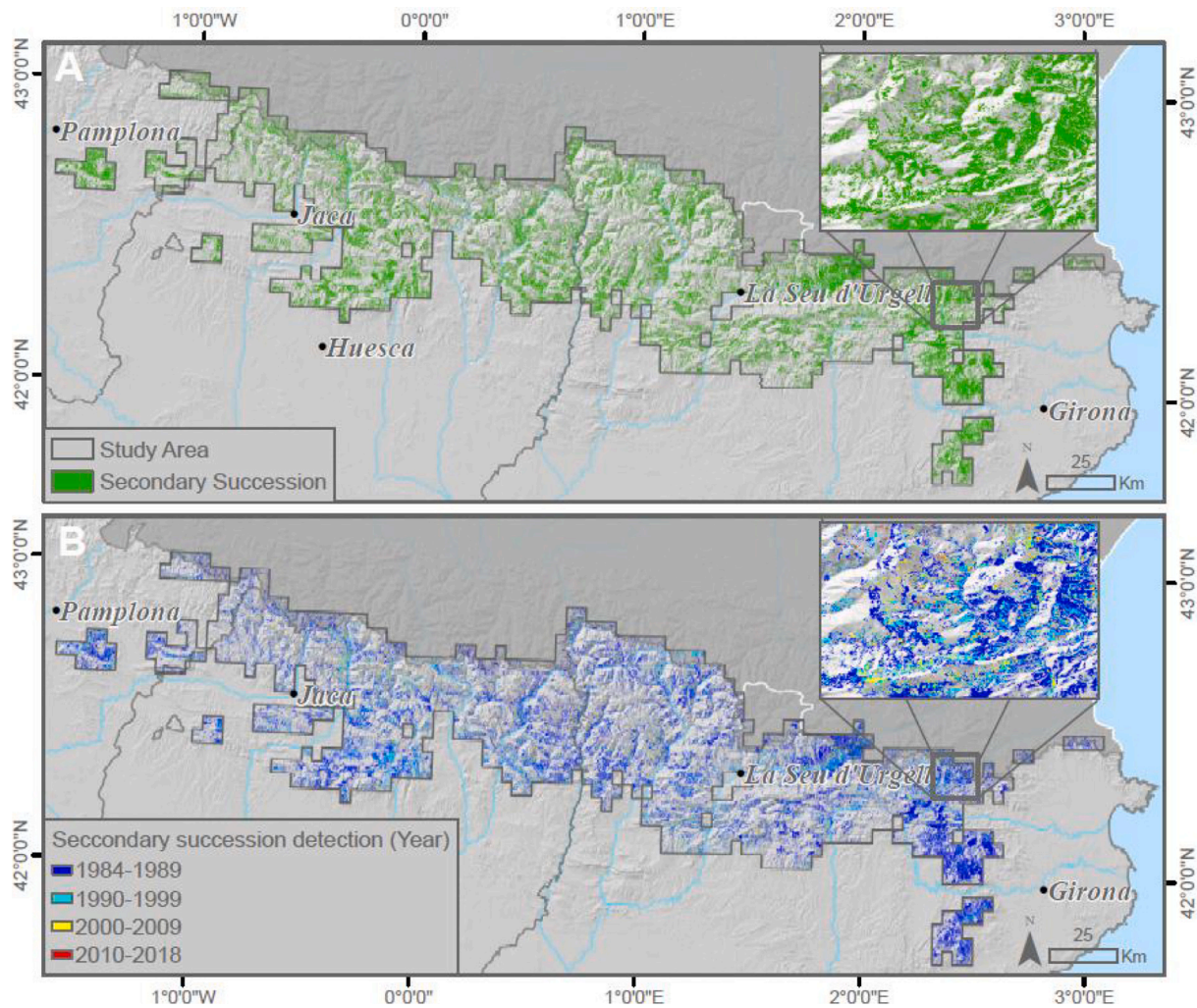
Fig. 4. a) Areas affected by SS using TC raw images; b) Areas affected by SS per year using TC raw images. Hillshade is used as background.
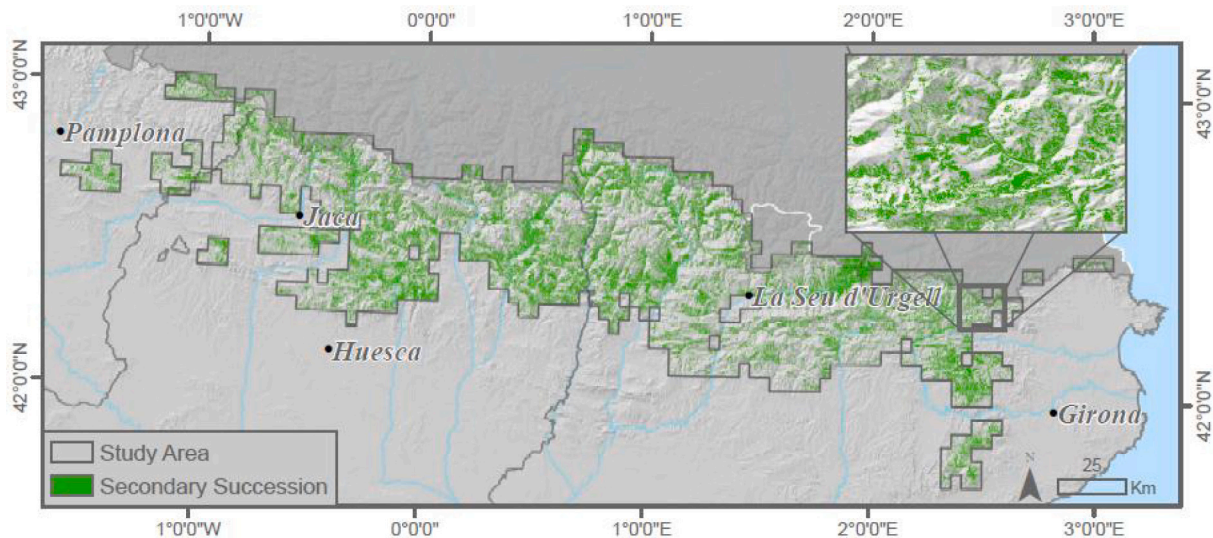

Fig. 5. Areas affected by SS using LT output images. Hillshade is used as background.

offer better results either. The TCA is an indirect measure of the proportion of vegetation in the pixel; the higher the TCA, the higher vegetation cover (Gómez et al., 2012). Since it largely refers to

vegetation cover, it holds low discriminant power to discern grassland from other vegetation covers.

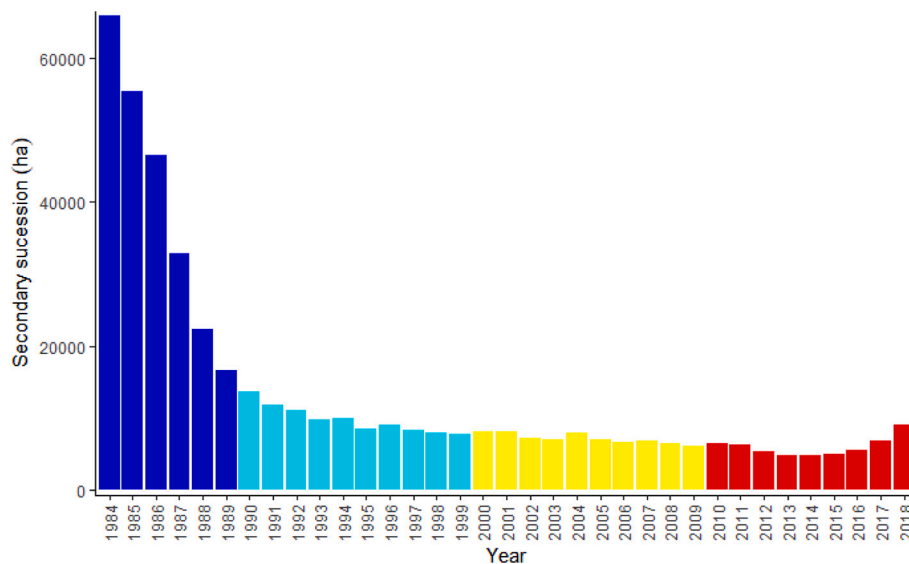When modeling the annual progression of SS, the temporal pattern

Fig. 6. Temporal evolution of SS. Colors represents the different decades.

obtained with LTTC was clearly different from TC Raw's. Setting aside the reported over commission of TC Raw models, their prediction of the year when SS started, i.e., the first detection of the transition from 'grasslands' to 'woody communities', was noticeably biased towards the beginning of the analysis period. Validation results confirmed the unreliable nature of the TC Raw's temporal distribution, in favor of the LTTC approach (AUCs of 0.83 and 0.75. respectively). Nonetheless, the temporal pattern obtained from LTTC also indicated higher SS rates during the first years, decreasing until the early 90s. The observed evolution afterwards points towards the stabilization of the progression of SS.

The temporal pattern described agrees with the literature in the topic. According to Lasanta and Vicente-Serrano (2007), the biggest changes associated to SS in the Pyrenees occurred between the 60s and 80s. Since 1990 there was a decreasing trend in forest expansion over grasslands and abandoned croplands (Vicente Serrano et al., 2003). Since the 19th to the mid-20th century, steep-sloped lands in mountain areas were cultivated (García-Ruiz et al., 2015). During the 1960 decade the Spanish Government funded many hydraulic infrastructures to promote agriculture in arid regions (Alonso-Sarría et al., 2016), leading to the decline in competitiveness of agricultural lands in mountain regions, the abandonment of croplands (van Leeuwen et al., 2019), and the decrease in population (moving mostly to cities in a pervasive rural exodus). During the rural exodus, due to reduced productivity, unsuitability for mechanization and poor accessibility, north-facing sites were abandoned first (Améztegui et al., 2010). After those, lands under steep slopes were progressively abandoned (García-Ruiz et al., 2015; Lasanta and Vicente-Serrano, 2007; Vicente Serrano et al., 2003). Nowadays agriculture in the Pyrenees remains mostly in the bottom of the mountain valleys (Lasanta et al., 2013). The promotion of recreational and touristic activities coupled to the low economic competitiveness of agriculture further favored land abandonment (van Leeuwen et al., 2019). This is also evidenced by the observed reduction in the number of goat and sheep cattle (INE, 2009; INE, 1999) and the increase in horse livestock, often used in recreational activities (Hjalager, 1996). In fact, these trends pose an additional challenge since goats are not forage selectors and therefore the greater presence of cows and horses selective grazing mainly consume the best forage (Sebastià et al., 2008). Despite the strong agreement with findings in the literature, a certain bias towards the first years might exist in our timing of SS. The PI helps in controlling potential temporal inconsistences, stabilizing the response of shrub encroachment over the whole time series, especially in middle-late temporal stages. However, several factors such as smoothing side-

effects LT predictors or the fact that we set the moment of change to the first year when SS was predicted, favors detection of SS at earlier stages.

The process of land abandonment followed by SS occurred with different intensities across the study region. Forest expansion produced by land abandonment had strong ecological consequences, both again positive and negative. In any case, the 64% reduction in managed grasslands and crops in the Spanish Pyrenees over the last 36 years implied a drastic decline in biodiversity and other ecosystem services linked to these valuable and fragile cultural landscapes.

6. Conclusions

The computational power and image collection of the Google Earth Engine platform joined to the implementation of the time-series harmonization algorithm LT allowed to estimate encroachment locations and timing in the Spanish Pyrenees for the last 36 years. Our results demonstrate the feasibility of the Landsat Tasseled Cap transformation time series, harmonized with LT (LTTC), to monitor annual SS in abandoned mountainous environments, using TCB and TCW in a SVM classification model. In general, non-harmonized time series offer worse performances and overestimate woodland expansion. Models using the LT outputs are also promising, but they do not offer temporal information on changes within the period of analysis.

Declaration of Competing Interest

The authors declare that they have no known competing financial interests or personal relationships that could have appeared to influence the work reported in this paper.

Appendix A. Supplementary data

Supplementary data to this article can be found online at https://doi.org/10.1016/j.rse.2021.112521.

References

Alcantara, C., Kuemmerle, T., Prishchepov, A.V., Radeloff, V.C., 2012. Mapping abandoned agriculture with multi-temporal MODIS satellite data. Remote Sens. Environ. 124, 334–347. https://doi.org/10.1016/j.rse.2012.05.019.

Ali, I., Cawkwell, F., Dwyer, E., Barrett, B., Green, S., 2016. Satellite remote sensing of grasslands: from observation to management. J. Plant Ecol. 9, 649–671. https://doi.org/10.1093/jpe/rtw005S.

Alonso-Sarría, F., Martínez-Hernández, C., Romero-Díaz, A., Cánovas-García, F., Gomariz-Castillo, F., 2016. Main environmental features leading to recent land abandonment in murcia region (Southeast Spain). L. Degrad. Dev. 27, 654–670. https://doi.org/10.1002/ldr.2447.

Améztegui, A., Brotons, L., Coll, L., 2010. Land-use changes as major drivers of mountain pine (*Pinus uncinata* Ram.) expansion in the Pyrenees. Glob. Ecol. Biogeogr. 19, 632–641. https://doi.org/10.1111/j.1466-8238.2010.00550.x.

Badia, A., Pèlachs, A., Vera, A., Tulla, A.F., Soriano, J.J., 2014. Land use and land cover change and the effects on vulnerability to forest fire of counties in the mountains of Catalonia: from managing the land to managing a threat. Pirineos 169. https://doi.org/10.3989/Pirineos.2014.169001.

Baumann, M., Kuemmerle, T., Elbakidze, M., Ozdogan, M., Radeloff, V.C., Keuler, N.S., Prishchepov, A.V., Kruhlov, I., Hostert, P., 2011. Patterns and drivers of post-socialist farmland abandonment in Western Ukraine. Land Use Policy. https://doi.org/10.1016/j.landusepol.2010.11.003.

Cervera, T., Pino, J., Marull, J., Padró, R., Tello, E., 2019. Understanding the long-term dynamics of forest transition: from deforestation to afforestation in a Mediterranean landscape (Catalonia, 1868–2005). Land Use Policy 80, 318–331. https://doi.org/10.1016/j.landusepol.2016.10.006.

Chinchor, N., 1992. MUC-4 evaluation metrics. In: Proceedings of the 4th Conference on Message Understanding, MUC4 '92. Association for Computational Linguistics, USA, pp. 22–29. https://doi.org/10.3115/1072064.1072067.

Cohen, W.B., Yang, Z., Healey, S.P., Kennedy, R., Gorelick, N., 2018. A LandTrendr multispectral ensemble for forest disturbance detection. Remote Sens. Environ. https://doi.org/10.1016/j.rse.2017.11.015.

Cortes, C., Vapnik, V., 1995. Support-vector networks. Mach. Learn. https://doi.org/10.1023/A:1022627411411.

Crist, E.P., 1985. A TM Tasseled Cap equivalent transformation for reflectance factor data. Remote Sens. Environ. https://doi.org/10.1016/0034-4257(85)90102-6.

Crist, E.P., Cicone, R.C., 1984. A physically-based transformation of thematic mapper data—the TM Tasseled Cap. IEEE Trans. Geosci. Remote Sens. https://doi.org/10.1109/TGRS.1984.350619.

Cuadrat, J.M., Saz, M.A., Vicente-Serrano, S.M., 2007. Atlas climático de Aragón. Gob. Aragón.

Estel, S., Kuemmerle, T., Alcántara, C., Levers, C., Prishchepov, A., Hostert, P., 2015. Mapping farmland abandonment and recultivation across Europe using MODIS NDVI time series. Remote Sens. Environ. 163, 312–325. https://doi.org/10.1016/j.rse.2015.03.028.

FAO, 2018. FAOSTAT statistical database. Crop. Natl. Prod.

Foley, J.A., DeFries, R., Asner, G.P., Barford, C., Bonan, G., Carpenter, S.R., Chapin, F.S., Coe, M.T., Daily, G.C., Gibbs, H.K., Helkowski, J.H., Holloway, T., Howard, E.A., Kucharik, C.J., Monfreda, C., Patz, J.A., Prentice, I.C., Ramankutty, N., Snyder, P.K., 2005. Global consequences of land use. Science (80-.) 309, 570–574. https://doi.org/10.1126/science.1111772.

Franklin, S.E., Ahmed, O.S., Wulder, M.A., White, J.C., Hermosilla, T., Coops, N.C., 2015. Large area mapping of annual land cover dynamics using multitemporal change detection and classification of landsat time series data. Can. J. Remote. Sens. 41, 293–314. https://doi.org/10.1080/07038992.2015.1089401.

Frazier, R.J., Coops, N.C., Wulder, M.A., 2015. Boreal Shield forest disturbance and recovery trends using Landsat time series. Remote Sens. Environ. 170, 317–327. https://doi.org/10.1016/j.rse.2015.09.015.

García Ruiz, J.M., Lasanta, T., 2018. El Pirineo Aragonés como paisaje cultural. Pirineos. https://doi.org/10.3989/pirineos.2018.173005.

García-Ruiz, J.M., López-Moreno, J.I., Lasanta, T., Vicente-Serrano, S.M., González-Sampériz, P., Valero-Garcés, B.L., Sanjuán, Y., Beguería, S., Nadal-Romero, E., Lana-Renault, N., Gómez-Villar, A., 2015. Los efectos geoecológicos del cambio global en el pirineo central español: Una revisión a distintas escalas espaciales y temporales. Pirineos 170. https://doi.org/10.3989/Pirineos.2015.170005.

Gartzia, M., Alados, C.L., Pérez-Cabello, F., 2014. Assessment of the effects of biophysical and anthropogenic factors on woody plant encroachment in dense and sparse mountain grasslands based on remote sensing data. Prog. Phys. Geogr. 38, 201–217. https://doi.org/10.1177/0309133314524429.

Gómez, C., White, J.C., Wulder, M.A., 2011. Characterizing the state and processes of change in a dynamic forest environment using hierarchical spatio-temporal segmentation. Remote Sens. Environ. https://doi.org/10.1016/j.rse.2011.02.025.

Gómez, C., Wulder, M.A., White, J.C., Montes, F., Delgado, J.A., 2012. Characterizing 25 years of change in the area, distribution, and carbon stock of Mediterranean pines in Central Spain. Int. J. Remote Sens. 33, 5546–5573. https://doi.org/10.1080/01431161.2012.663115.

Gorelick, N., Hancher, M., Dixon, M., Ilyushchenko, S., Thau, D., Moore, R., 2017. Google Earth Engine: planetary-scale geospatial analysis for everyone. Remote Sens. Environ. https://doi.org/10.1016/j.rse.2017.06.031.

Healey, S.P., Cohen, W.B., Zhiqiang, Y., Krankina, O.N., 2005. Comparison of Tasseled Cap-based Landsat data structures for use in forest disturbance detection. Remote Sens. Environ. 97, 301–310. https://doi.org/10.1016/j.rse.2005.05.009.

Hijmans, R.J., 2019. raster: Geographic Data Analysis and Modeling.

Hjalager, A.-M., 1996. Agricultural diversification into tourism. Tour. Manag. https://doi.org/10.1016/0261-5177(95)00113-1.

Huang, C., Goward, S.N., Masek, J.G., Thomas, N., Zhu, Z., Vogelmann, J.E., 2010. An automated approach for reconstructing recent forest disturbance history using dense Landsat time series stacks. Remote Sens. Environ. https://doi.org/10.1016/j.rse.2009.08.017.

INE, 1999. Censo Agrario.

INE, 2009. Censo Agrario.

José Vidal-Macua, J., Ninyerola, M., Zabala, A., Domingo-Marimon, C., Pons, X., 2017. Factors affecting forest dynamics in the Iberian Peninsula from 1987 to 2012. The role of topography and drought. For. Ecol. Manag. 406, 290–306. https://doi.org/10.1016/j.foreco.2017.10.011.

Kennedy, R., Yang, Z., Cohen, W.B., 2010. Detecting trends in forest disturbance and recovery using yearly Landsat time series: 1. LandTrendr - temporal segmentation algorithms. Remote Sens. Environ. https://doi.org/10.1016/j.rse.2010.07.008.

Kennedy, R., Yang, Z., Cohen, W.B., Pfaff, E., Braaten, J., Nelson, P., 2012. Spatial and temporal patterns of forest disturbance and regrowth within the area of the Northwest Forest Plan. Remote Sens. Environ. https://doi.org/10.1016/j.rse.2011.09.024.

Kennedy, R., Yang, Z., Gorelick, N., Braaten, J., Cavalcante, L., Cohen, W.B., Healey, S., 2018. Implementation of the LandTrendr algorithm on Google Earth Engine. Remote Sens. https://doi.org/10.3390/rs10050691.

Kuemmerle, T., Hostert, P., Radeloff, V.C., Van Der Linden, S., Perzanowski, K., Kruhlov, I., 2008. Cross-border comparison of post-socialist farmland abandonment in the Carpathians. Ecosystems 11, 614–628. https://doi.org/10.1007/s10021-008-9146-z.

Kuemmerle, T., Chaskovskyy, O., Knorn, J., Radeloff, V.C., Kruhlov, I., Keeton, W.S., Hostert, P., 2009. Forest cover change and illegal logging in the Ukrainian Carpathians in the transition period from 1988 to 2007. Remote Sens. Environ. 113, 1194–1207. https://doi.org/10.1016/j.rse.2009.02.006.

Kuhn, M., 2008. Building predictive models in R using the caret package. J. Stat. Softw. 28, 1–26.

Lahsen, M., Sanchez-Rodriguez, R., Lankao, P.R., Dube, P., Leemans, R., Gaffney, O., Mirza, M., Pinho, P., Osman-Elasha, B., Smith, M.S., 2010. Impacts, adaptation and vulnerability to global environmental change: Challenges and pathways for an action-oriented research agenda for middle-income and low-income countries. Curr. Opin. Environ. Sustain. https://doi.org/10.1016/j.cosust.2010.10.009.

Lal, R., 2004. Soil carbon sequestration impacts on global climate change and food security. Science (80-.). https://doi.org/10.1126/science.1097396.

Lasanta, T., Vicente-Serrano, S.M., 2007. Cambios en la cubierta vegetal en el pirineo aragonés en los últimos 50 años. Pirineos 125–154. https://doi.org/10.3989/pirineos.2007.v162.16.

Lasanta, T., Beltran, O., Vaccaro, I., 2013. Socioeconomic and territorial impact of the ski industry in the spanish pyrenees: mountain development and leisure induced urbanization. Pirineos 168, 103–128. https://doi.org/10.3989/Pirineos.2013.168006.

Lasanta, T., Arnáez, J., Pascual, N., Ruiz-Flaño, P., Errea, M.P., Lana-Renault, N., 2017. Space–time process and drivers of land abandonment in Europe. Catena 149, 810–823. https://doi.org/10.1016/j.catena.2016.02.024.

Lasanta, T., Khorchani, M., Pérez-Cabello, F., Errea, P., Sáenz-Blanco, R., Nadal-Romero, E., 2018. Clearing shrubland and extensive livestock farming: active prevention to control wildfires in the Mediterranean mountains. J. Environ. Manag. 227, 256–266. https://doi.org/10.1016/j.jenvman.2018.08.104.

Latham, J., Cumani, R., Rosati, I., Bloise, M., 2014. FAO Global Land Cover SHARE. Database Beta-release Verion 1.0.

Matthews, B.W., 1975. Comparison of the predicted and observed secondary structure of T4 phage lysozyme. Biochim. Biophys. Acta 405, 442–451. https://doi.org/10.1016/0005-2795(75)90109-9.

Mottet, A., Ladet, S., Coqué, N., Gibon, A., 2006. Agricultural land-use change and its drivers in mountain landscapes: a case study in the Pyrenees. Agric. Ecosyst. Environ. https://doi.org/10.1016/j.agee.2005.11.017.

Navarro, L.M., Pereira, H.M., 2012. Rewilding abandoned landscapes in Europe. Ecosystems. https://doi.org/10.1007/s10021-012-9558-7.

Noi, P.T., Kappas, M., 2018. Comparison of random forest, k-nearest neighbor, and support vector machine classifiers for land cover classification using sentinel-2 imagery. Sensors 18 (1). https://doi.org/10.3390/s18010018.

O'Mara, F.P., 2012. The role of grasslands in food security and climate change. Ann. Bot. 110, 1263–1270. https://doi.org/10.1093/aob/mcs209.

Pausas, J.G., Bond, W.J., 2020. Alternative biome states in terrestrial ecosystems. Trends Plant Sci. 1–14. https://doi.org/10.1016/j.tplants.2019.11.003.

Pickell, P.D., Hermosilla, T., Frazier, R.J., Coops, N.C., Wulder, M.A., 2016. Forest recovery trends derived from Landsat time series for North American boreal forests. Int. J. Remote Sens. 37, 138–149. https://doi.org/10.1080/2150704X.2015.1126375.

PNOA, 2019. Plan Nacional de Ortofotografía Aérea. Ministerio de Transporte Movilidad y Agenda Urbana. https://pnoa.ign.es/presentacion-y-objetivo.

Poyatos, R., Latron, J., Llorens, P., 2003. Land use and land cover change after agricultural abandonment. Mt. Res. Dev. 23, 362–368. https://doi.org/10.1659/0276-4741(2003)023[0362:lualcc]2.0.co;2.

R Core Team, 2017. R: A Language and Environment for Statistical Computing.

Rodrigues, M., de la Riva, J., 2014. An insight into machine-learning algorithms to model human-caused wildfire occurrence. Environ. Model. Softw. 57, 192–201.

Roy, D.P., Kovalskyy, V., Zhang, H.K., Vermote, E.F., Yan, L., Kumar, S.S., Egorov, A., 2016. Characterization of Landsat-7 to Landsat-8 reflective wavelength and normalized difference vegetation index continuity. Remote Sens. Environ. 185, 57–70. https://doi.org/10.1016/j.rse.2015.12.024.

Sebastià, M.T., De Bello, F., Puig, L., Taull, M., 2008. Grazing as a factor structuring grasslands in the Pyrenees. Appl. Veg. Sci. https://doi.org/10.3170/2008-7-18358.

Senf, C., Pflugmacher, D., Wulder, M.A., Hostert, P., 2015. Characterizing spectral-temporal patterns of defoliator and bark beetle disturbances using Landsat time series. Remote Sens. Environ. https://doi.org/10.1016/j.rse.2015.09.019.

SIOSE, 2014. Sistema de Información de Ocupación del Suelo en España. Technical report. Ministerio de Fomento. https://www.siose.es/SIOSEtheme-theme/document os/pdf/Doc_tec_SIOSE2014_v1.pdf.

Sørensen, M.V., Strimbeck, R., Nystuen, K.O., Kapas, R.E., Enquist, B.J., Graae, B.J., 2018. Draining the pool? Carbon storage and fluxes in three alpine plant communities. Ecosystems. https://doi.org/10.1007/s10021-017-0158-4.

Tanase, M.A., de las Heras, J., Santoro, M., Pérez-Cabello, F., Kasischke, E., 2011. Sensitivity of SAR data to post-fire forest regrowth in Mediterranean and boreal forests. Remote Sens. Environ. 115, 2075–2085.

Turner, B.L.I.I., Meyer, W.B., Skole, D.L., 1994. Global land-use/land-cover change: towards an integrated study. Ambio 23, 91–95. https://doi.org/10.2307/4314168.

Ustaoglu, E., Collier, M.J., 2018. Farmland abandonment in Europe: an overview of drivers, consequences, and assessment of the sustainability implications. Environ. Rev. 26, 396–416. https://doi.org/10.1139/er-2018-0001.

Vacquie, L., Houet, T., Sohl, T., Reker, R., Sayler, K., 2015. Modelling regional land change scenarios to assess land abandonment and reforestation dynamics in the Pyrenees (France). J. Mt. Sci. 12, 905–920.

Van Auken, O.W., 2009. Causes and consequences of woody plant encroachment into western North American grasslands. J. Environ. Manag. https://doi.org/10.1016/j.jenvman.2009.04.023.

van Leeuwen, C.C.E., Cammeraat, E.L.H., de Vente, J., Boix-Fayos, C., 2019. The evolution of soil conservation policies targeting land abandonment and soil erosion in Spain: a review. Land Use Policy 83, 174–186. https://doi.org/10.1016/j.landusepol.2019.01.018.

Vapnik, V., 1995. The Nature of Statistical Learning Theory. https://doi.org/10.1007/978-1-4757-2440-0.

Vapnik, V., 1998. Statistical Learning Theory. Wiley, New York.

Vicente Serrano, S.M., Lasanta, T., Romo, A., 2003. Diferencias espaciales en la evolución del NDVI en la cuenca alta del Aragón : efectos de los caminos en el uso del suelo. Cuad. Investig. Geogr. 29, 51. https://doi.org/10.18172/cig.1058.

Vicente-Serrano, S.M., Beguería, S., Lasanta, T., 2006. Diversidad espacial de la actividad vegetal en campos abandonados del pirineo central español: Análisis de los procesos de sucesión mediante imágenes landsat (1984–2001). Pirineos 59–84.

Vila Subirós, J., Ribas Palom, A., Varga Linde, P., Llausàs Pascual, A., 2009. Medio siglo de cambios paisajísticos en la montaña mediterránea. Percepción y valoración social del paisaje en la alta Garrotxa (Girona). Pirineos 164. https://doi.org/10.3989/pirineos.2009.v164.30.

Zhu, Z., Woodcock, C.E., 2014. Continuous change detection and classification of land cover using all available Landsat data. Remote Sens. Environ. https://doi.org/10.1016/j.rse.2014.01.011.